Confocal microscopy with a radially polarized focused beam

Meng, Peiwen; Pereira, Silvania; Urbach, Paul

DOI
10.1364/OE.26.029600

Publication date
2018

Document Version
Final published version

Published in
Optics Express

Research Article | Vol. 26, No. 23 | 12 Nov 2018 | OPTICS EXPRESS 29600

Optics EXPRESS

Confocal microscopy with a radially polarized focused beam

Peiwen Meng,* Silvania Pereira, and Paul Urbach

Optics Research Group, Department of Imaging Physics, Delft University of Technology, Lorentzweg 1, 2628 CJ Delft, Netherlands
*P.Meng@tudelft.nl

Abstract: Rigorous vectorial focusing theory is used to study the imaging of small adjacent particles with a confocal laser scanning system. We consider radially polarized illumination with an optimized amplitude distribution and an annular lens to obtain a narrower distribution of the longitudinal component of the field in focus. A polarization convertor at the detector side is added to transform radial polarization to linear polarization in order to make the signal detectable with a single mode fiber.

1. Introduction

Many super-resolution microscopes such as STED [1], PALM [2], and STORM [3] have become very important in science and applications because of their high quality images. While the applications of these super-resolution microscopy are attractive, there are some disadvantages like extremely expensive systems, time-consuming data acquisition and choices of fluorescent dyes, which limit the techniques in some cases. Although the lateral resolution of conventional confocal imaging systems is limited because of the diffraction limit, confocal microscopy has a wide range of applications in the biological and medical sciences [4–6], as well as nano-crystal imaging and spectroscopy [7, 8]. Thus, the development of a cheap and simplified confocal system combined with super-resolution imaging is very attractive.

The total point spread function (PSF) of the confocal system is determined by both the excitation PSF and the detection PSF, where the former is related to the focused illumination and the latter depends on the small pinhole or a fiber in the detector plane [9]. A very small pinhole which can remove the out of focus information plays an important role in improving both the axial and lateral resolutions in confocal microscopy. Wilson [10] compares the images theoretically and experimentally of scatterers using conventional and confocal microscopes. However, only linearly and circularly polarized beams are considered there. Cylindrical vector beams are well-established tools in optics because of the applicability of radially polarized beams in several areas. For example, using radially polarized light, the longitudinal electric component of the illuminating focused spot can be made small [11–13]. Provided the sample interacts only with the longitudinal component, higher resolution can be obtained. For a high numerical aperture (NA) system, and a radially polarized pupil field, the longitudinal component can be enhanced compared to the transverse component by using an annular aperture in the pupil of the focusing objective. The latter also results in a tighter focusing spot size of the longitudinal component in the focal plane [14–16], although this is at the expense of stronger sidelobes which will reduce the imaging quality. However, annular apertures do not give the largest longitudinal component in focus. Other pupil filter functions, for example, a BOE [17–20], a parabolic mirror and a flat diffractive lens [21] are proposed to achieve sharper focal spot sizes and as a consequence, higher resolution. By shaping the radially polarized pupil field such that the amplitude increases monotonically in a specific way as function of the pupil radius, the full-width-at-half-maximum (FWHM) of the intensity of longitudinal component reaches a value that is 15% to 30% lower than that of the spot of a focused linear polarized pupil field [22]. Spot-size reduction by means of

#340629 https://doi.org/10.1364/OE.26.029600
Journal © 2018 Received 25 Jul 2018; revised 15 Sep 2018; accepted 15 Sep 2018; published 29 Oct 2018

Optics EXPRESS

focusing the optimized radially polarized light is shown experimentally according to theoretical productions [23]. However, in a confocal configuration, when strong longitudinal field excites a longitudinal sensitive sample, for example, a dipole is oriented parallel to the optical axis, the consequence is that its image with low NA that is formed at the pinhole side has a zero at the center [24]. In order to make the signal detectable, a polarization convertor placed in the path of detection plane is proposed to engineer the detection PSF from a doughnut shape to one with maximum in the center [25]. In the reference [26], good imaging results are achieved with the confocal microscope together with a polarization convertor experimentally. However, the theoretical analysis of the entire system is not complete.

In this paper, we present a fully rigorous vectorial theory to describe the whole confocal imaging process in a high NA system with spatially shaped radially polarized illumination. The optimized pupil field which maximizes the longitudinal electric field component in the focal point [22] is compared with the linearly polarized and traditional radially polarized pupil field to validate that the former one gives higher lateral resolution. The annular pupil field with radially polarized illumination is also considered. We use two longitudinally oriented electric dipoles at variable distances as test object. Other orientations can be easily considered. A suitable pinhole size is chosen before the detector plane to enhance the system performance, and a polarization convertor is inserted in the collimated optical path before the pinhole to transform the radially polarized light scattered by the object back to linearly polarized light to optimize the power of the light after the pinhole.

2. Theoretical analysis

In scalar diffraction theory the focal field of a lens is considered without taking into account the vectorial nature of the light field. However, the scalar method is not valid for optical systems of high NA that we study in this paper and vectorial theory is needed to describe the field near the focal plane. Originating from Ignatovsky's diffraction theory [27], later studied in detail in [28, 29], the solution is referred as the vectorial Richard-Wolf integral.

Rigorous analysis of vectorial image formation in the confocal system can be found in [9]. In this paper we consider different polarizations and optimized pupil field for the illumination. Fig. 1(a) shows the configuration of the confocal imaging system. In order to make the whole analytical process clear, we consider first the focusing spot which illuminates the sample. This focused spot excites electric dipoles in the sample which are then imaged on the detector. The imaging of the excited dipoles is studied in subsequent sections. All optical fields that we consider in this paper are time harmonic with time dependence given by the factor $\exp(-i\omega t)$, where $\omega > 0$ is the frequency. This factor is omitted from all formulas below.

2.1. Dipole excitation using a focused spot

Figure 1(b) describes the process of focusing the illumination beam by lens L_1. This focused field subsequently excites electric dipoles in the sample. We choose a coordinate system (x, y, z) with z-axis coinciding with the optical axis and origin at the Gaussian focal point of lens L_1 and such that the illuminating beam propagates in the positive z-direction. When focused in a homogeneous medium with real refractive index n, the electric and magnetic fields in the focal region of lens L_1 can be expanded into plane waves:

$$\begin{aligned}\mathbf{E}^e(\mathbf{r}) &= \frac{1}{4\pi^2}\iint_{k_\perp \le k_0 \mathrm{NA}_1} \mathbf{A}(\mathbf{k}_\perp)\exp(i\mathbf{k}\cdot\mathbf{r})d^2k_\perp,\\ \mathbf{H}^e(\mathbf{r}) &= \frac{1}{4\pi^2}\frac{1}{\omega\mu_0}\iint_{k_\perp \le k_0 \mathrm{NA}_1} \mathbf{k}\times\mathbf{A}(\mathbf{k}_\perp)\exp(i\mathbf{k}\cdot\mathbf{r})d^2k_\perp,\end{aligned} \tag{1}$$

Optics EXPRESS

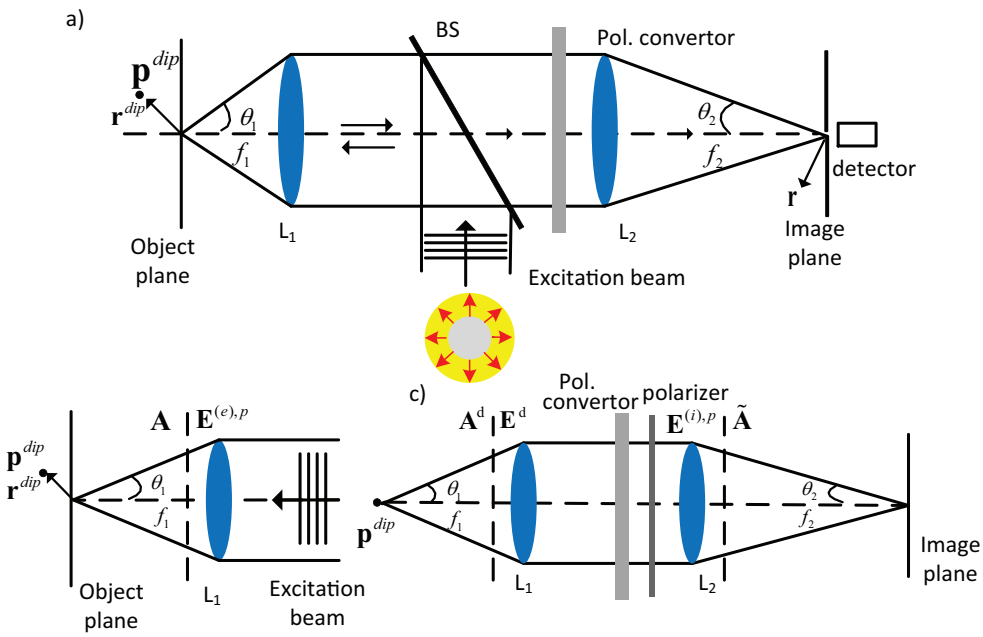

Fig. 1. Schematic of the confocal microscope. A beam splitter divides the excitation path and detection path into two arms. A laser beam is focused onto the sample by a high NA objective lens L_1. The light scattered by the sample is collected by the same objective lens and focused by a small NA lens onto a pinhole in front of a detector. a) The complete confocal microscopy system, b) Focusing and dipole excitation, c) Imaging and polarization conversion.

where $\vec{\mathbf{A}}(\vec{\mathbf{k}})$ is the vector amplitude of the plane wave with the wave vector $\vec{\mathbf{k}} = (k_x, k_y, k_z)$, $\mathbf{k}_\perp = (k_x, k_y)$ is the part of the wave vector perpendicular to the optical axis, with $k_\perp = \sqrt{k_x^2 + k_y^2}$ its length, $k_z = \sqrt{k^2 - k_\perp^2}$, where $k = k_0 n$ with $k_0 = 2\pi/\lambda_0$ with λ_0 the wavelength in vacuum. Note that the transverse wavenumber $k_\perp$ satisfies: $0 \le k_\perp \le k_0 \mathrm{NA}_1$, where $\mathrm{NA}_1 = n \sin\theta_{\max}^{(1)}$ with $\theta_{\max}^{(1)}$ the maximum angle between the wave vectors and the positive z direction.

To define the polarizations of the plane waves, we define a positively oriented orthonormal basis $\widehat{\mathbf{k}}, \widehat{\mathbf{p}}, \widehat{\mathbf{s}}$ in reciprocal $\mathbf{k}-$space by:

$$\begin{aligned}
\widehat{\mathbf{k}} &= \frac{k_x}{k}\widehat{\mathbf{x}} + \frac{k_y}{k}\widehat{\mathbf{y}} + \frac{k_z}{k}\widehat{\mathbf{z}}, \\
\widehat{\mathbf{p}}(\mathbf{k}_\perp) &= \frac{k_x k_z \widehat{\mathbf{x}} + k_y k_z \widehat{\mathbf{y}} - (k_x^2 + k_y^2)\widehat{\mathbf{z}}}{k\sqrt{{k_x}^2 + {k_y}^2}}, \\
\widehat{\mathbf{s}}(\mathbf{k}_\perp) &= \frac{-k_y \widehat{\mathbf{x}} + k_x \widehat{\mathbf{y}}}{\sqrt{{k_x}^2 + {k_y}^2}},
\end{aligned} \tag{2}$$

Since the electric field is free of divergence, the vector amplitude $\mathbf{A}$ can be written as:

$$\mathbf{A}(\mathbf{k}_\perp) = A_\mathrm{p}(\mathbf{k}_\perp)\widehat{\mathbf{p}}(\mathbf{k}_\perp) + A_\mathrm{s}(\mathbf{k}_\perp)\widehat{\mathbf{s}}(\mathbf{k}_\perp), \tag{3}$$

Optics EXPRESS

where A_p and A_s are the components of $\mathbf{A}$ on the basis of $\widehat{\mathbf{p}}, \widehat{\mathbf{s}}$.

The electromagnetic field in focus can be therefore rewritten as:

$$\begin{aligned}\mathbf{E}^e(\mathbf{r}) &= \frac{1}{4\pi^2}\iint_{k_\perp \le k_0 \mathrm{NA}_1} \left(A_\mathrm{p}\widehat{\mathbf{p}} + A_\mathrm{s}\widehat{\mathbf{s}}\right) e^{i\mathbf{k}\cdot\mathbf{r}} d^2k_\perp,\\ \mathbf{H}^e(\mathbf{r}) &= \frac{1}{4\pi^2}\frac{1}{\omega\mu_0}\iint_{k_\perp \le k_0 \mathrm{NA}_1} \left(-A_\mathrm{s}\widehat{\mathbf{p}} + A_\mathrm{p}\widehat{\mathbf{s}}\right) e^{i\mathbf{k}\cdot\mathbf{r}} d^2k_\perp.\end{aligned} \tag{4}$$

According to the vectorial diffraction theory [27–29], the plane wave amplitudes $A_\mathrm{p}, A_\mathrm{s}$ are linked to the radial and azimuthal components of the pupil field by:

$$A_\mathrm{p}(\mathbf{k}_\perp) = \frac{2\pi i f_1}{\sqrt{k k_z}}\mathrm{E}_\rho^{e,p}(\rho_p, \varphi_p), \quad A_\mathrm{s}(\mathbf{k}_\perp) = \frac{2\pi i f_1}{\sqrt{k k_z}}\mathrm{E}_\varphi^{e,p}(\rho_p, \varphi_p), \tag{5}$$

where, f_1 is the focal distance of the objective lens L_1 and ρ_p, φ_p are polar pupil coordinates defined by:

$$\rho_p = f_1\frac{k_\perp}{k_0 n}, \quad \rho_p\cos\varphi_p = -f_1\frac{k_x}{k_0 n}, \quad \rho_p\sin\varphi_p = -f_1\frac{k_y}{k_0 n}, \tag{6}$$

Note that

$$\cos\varphi_p = -k_x/k_\perp, \quad \sin\varphi_p = -k_y/k_\perp. \tag{7}$$

Next we consider the focusing of two pupil fields in more details.

2.1.1. Focusing of a linear polarized pupil field

When the pupil field is in all points of the pupil linearly polarized parallel to the x-direction, we have:

$$E_\rho^{e,p}(\rho_p, \varphi_p) = g(\rho_p)\cos\varphi_p, \quad E_\varphi^{e,p}(\rho_p, \varphi_p) = g(\rho_p)\sin\varphi_p, \tag{8}$$

where $g(\rho_p)$ is the amplitude which may be a function of the radius. Using Eq. (7), we get:

$$A_\mathrm{p}(\mathbf{k}_\perp) = \frac{-2\pi i f_1 k_x}{\sqrt{k k_z}k_\perp}g(k_\perp), \quad A_\mathrm{s}(\mathbf{k}_\perp) = \frac{-2\pi i f_1 k_y}{\sqrt{k k_z}k_\perp}g(k_\perp), \tag{9}$$

where for brevity, we have written $g(k_\perp)$ instead of $g(f_1 k_\perp/k)$.

We substitute Eq. (9) into Eq. (4) and use the following integrals [30]:

$$\begin{aligned}\int_0^{2\pi}\cos n\phi e^{ix\cos(\phi-\varphi)}d\phi &= 2\pi i^n \mathrm{J}_n(x)\cos n\varphi,\\ \int_0^{2\pi}\sin n\phi e^{ix\cos(\phi-\varphi)}d\phi &= 2\pi i^n \mathrm{J}_n(x)\sin n\varphi,\end{aligned} \tag{10}$$

where $\mathrm{J}_n(x)$ is the Bessel function of nth order. By using cylindrical coordinates in the focal region, we then obtain for the electric field in the focal region:

$$\mathbf{E}^e(\rho, \varphi, z) = \frac{-i f_1}{2k^{3/2}}\begin{pmatrix} -I_{00}(\rho, z) - I_{02}(\rho, z)\cos 2\varphi \\ -I_{02}(\rho, z)\sin 2\varphi \\ 2iI_{01}(\rho, z)\cos\varphi \end{pmatrix}, \tag{11}$$

Optics EXPRESS

where

$$I_{00}(\rho, z) = \int_0^{k_0 \mathrm{NA}_1} g(k_\perp)\,(k + k_z)\,\mathrm{J}_0(k_\perp \rho)\frac{k_\perp}{\sqrt{k_z}} e^{ik_z z} dk_\perp, \tag{12}$$

$$I_{01}(\rho, z) = \int_0^{k_0 \mathrm{NA}_1} g(k_\perp) k_\perp \mathrm{J}_1(k_\perp \rho)\frac{k_\perp}{\sqrt{k_z}} e^{ik_z z} dk_\perp, \tag{13}$$

$$I_{02}(\rho, z) = \int_0^{k_0 \mathrm{NA}_1} g(k_\perp)\,(k - k_z)\,\mathrm{J}_2(k_\perp \rho)\frac{k_\perp}{\sqrt{k_z}} e^{ik_z z} dk_\perp. \tag{14}$$

2.1.2. Focusing of a radially polarized pupil field

For a pupil field which is in all points of the pupil polarized in the radial direction, the radial and azimuthal components of the electric pupil field are given by:

$$E_\rho^{e,p}(\rho_p, \varphi_p) = g(\rho_p), \quad E_\varphi^{e,p}(\rho_p, \varphi_p) = 0, \tag{15}$$

where the amplitude g is a function of the pupil radius. By using Eq.(5), we get for the p- and s-components of the electric field of the plane waves in the focal region:

$$A_\mathrm{p}(\mathbf{k}_\perp) = \frac{2\pi i f_1}{\sqrt{k k_z}} g(k_\perp), \quad A_\mathrm{s}(\mathbf{k}_\perp) = 0, \tag{16}$$

where (as above) we have written $g(k_\perp)$ instead of the formally more correct $g\,(f_1 k_\perp / k)$. Then with Eq. (4) and the integrals of Eq. (10), the electric field in the focal region becomes in terms of cylindrical coordinates:

$$\mathbf{E}^e(\rho, \varphi, z) = \frac{-f_1}{k^{3/2}} \begin{pmatrix} I_{11}(\rho, z)\cos\varphi \\ I_{11}(\rho, z)\sin\varphi \\ i I_{10}(\rho, z) \end{pmatrix}, \tag{17}$$

where

$$I_{10}(\rho, z) = \int_0^{k_0 \mathrm{NA}_1} g(k_\perp) k_\perp \mathrm{J}_0(k_\perp \rho)\frac{k_\perp}{\sqrt{k_z}} e^{ik_z z} dk_\perp, \tag{18}$$

$$I_{11}(\rho, z) = \int_0^{k_0 \mathrm{NA}_1} g(k_\perp) k_z \mathrm{J}_1(k_\perp \rho)\frac{k_\perp}{\sqrt{k_z}} e^{ik_z z} dk_\perp. \tag{19}$$

We discuss now two special radially polarized pupil fields. The first is the pupil field derived in [22] which gives the largest possible longitudinal (i.e. z-component) of the electric field component in the focal point, for a given power P_0 in the pupil of the lens. This solution makes the longitudinal component of the focused electric field quite narrow. It was shown in [22] that the amplitude of this optimum pupil field is given by:

$$g(k_\perp) = -\frac{k_\perp^{3/2} k^{1/2}}{2\pi i f_1 k_z \Lambda}, \tag{20}$$

where

$$\Lambda = \left(\frac{\pi}{\mathrm{P}_0}\right)^{1/2} \frac{n^{1/2}}{\lambda_0} \left(\frac{\epsilon_0}{\mu_0}\right)^{1/4} \left(\frac{2}{3} - \sqrt{1 - (\mathrm{NA}_1/n)^2} + \frac{1}{3}\sqrt{\left(1 - (\mathrm{NA}_1/n)^2\right)^3}\right)^{1/2}, \tag{21}$$

Optics EXPRESS

By substituting Eq. (20), Eqs. (18) and (19) become:

$$I_{10}(\rho, z) = -\frac{k^{1/2}}{2\pi i f_1 \Lambda} \int_0^{k_0 \mathrm{NA}_1} \mathrm{J}_0(k_\perp \rho) \frac{k_\perp^{7/2}}{k_z^{3/2}} e^{ik_z z} dk_\perp, \tag{22}$$

$$I_{11}(\rho, z) = -\frac{k^{1/2}}{2\pi i f_1 \Lambda} \int_0^{k_0 \mathrm{NA}_1} \mathrm{J}_1(k_\perp \rho) \frac{k_\perp^{5/2}}{k_z^{3/2}} e^{ik_z z} dk_\perp. \tag{23}$$

The second choice for the amplitude g of the radially polarized pupil field which gives a narrow longitudinal component in the focal plane corresponds to an annular pupil:

$$g(\rho_p) = \begin{cases} 1 & a - \Delta\rho_p < \rho_p \leq a \\ 0 & \text{otherwise} \end{cases}, \tag{24}$$

where a is the radius of the pupil of the lens L_1 and $\Delta\rho_p$ is the width of the annular ring. Then the focal field is obtained by substituting Eq. (24) for g in Eqs. (17)-(19). As we will show in Section 3, the longitudinal component in the focal plane of the annular pupil is narrower than the optimized pupil amplitude in Eq. (20) and becomes more narrower for smaller width $\Delta\rho_p$ of the annular pupil aperture. However, the annular pupil field has the disadvantage that for a very small annular aperture, there is only little energy in the focal region.

2.2. Imaging without a polarization convertor

Figure 1(c) shows the imaging part of the optical system. In the Born approximation, the focused field $\mathbf{E}^i$ excites a dipole density $\mathbf{P}^d(\mathbf{r}_d)$ at the position $\mathbf{r}_d = (x_d, y_d, z = 0)$, where the $z = 0$ plane is, as before, assumed to coincide with the focal plane of lens L_1. The dipole vector is given by:

$$\mathbf{P}^d = \overleftrightarrow{\alpha} \mathbf{E}^e(\mathbf{r}_d), \tag{25}$$

where $\overleftrightarrow{\alpha}$ is the electric polarizability. It in general is a tensor, and we assume that the tensor has principal axis that are parallel to the x, y, z−axis, i.e

$$\overleftrightarrow{\alpha} = \begin{pmatrix} \alpha_{xx} & 0 & 0 \\ 0 & \alpha_{yy} & 0 \\ 0 & 0 & \alpha_{zz} \end{pmatrix}. \tag{26}$$

Let $\mathbf{E}^d$ be the electric field radiated by this dipole. Its plane wave amplitudes in the entrance pupil of lens L_1, i.e. for $z = f_1$, are given by [31]:

$$A^d(\mathbf{k}_\perp) = -\frac{e^{ik_z f_1}}{2i\epsilon_0 n^2 k_z} \mathbf{k} \times (\mathbf{k} \times \mathbf{P}^d), \tag{27}$$

Hence,

$$A_\mathrm{p}^d(\mathbf{k}_\perp) = \frac{e^{ik_z f_1}}{2i\epsilon_0 n^2 k_z} k^2 \mathbf{P}^d \cdot \widehat{\mathbf{p}}, \quad A_\mathrm{s}^d(\mathbf{k}_\perp) = \frac{e^{ik_z f_1}}{2i\epsilon_0 n^2 k_z} k^2 \mathbf{P}^d \cdot \widehat{\mathbf{s}}, \tag{28}$$

Using Eq. (5) and (6), the radial and azimuthal components of the pupil field are:

$$E_\rho^{d,p}(\rho_p, \varphi_p) = \frac{\sqrt{k k_z}}{2\pi i f_1} A_\mathrm{p}^d(\mathbf{k}_\perp), \quad E_\varphi^{d,p}(\rho_p, \varphi_p) = \frac{\sqrt{k k_z}}{2\pi i f_1} A_\mathrm{s}^d(\mathbf{k}_\perp). \tag{29}$$

Optics EXPRESS

The refocusing by the second lens L_2 with focal length f_2 yields plane wave amplitudes in image space which are given by

$$\begin{aligned}\tilde{A}_{\mathrm{p}}^{d}(\tilde{\mathbf{k}}_{\perp}) &= \frac{2\pi i f_2}{\sqrt{k\tilde{k}_z}}\mathrm{E}_{\rho}^{d,p}(\rho_p,\varphi_p) = \frac{f_2}{f_1}\sqrt{\frac{k_z}{\tilde{k}_z}}\frac{e^{ik_z f_1}}{2i\epsilon_0 n^2 k_z}k^2\mathbf{P}^d\cdot\widehat{\mathbf{p}},\\ \tilde{A}_{\mathrm{s}}^{d}(\tilde{\mathbf{k}}_{\perp}) &= \frac{2\pi i f_2}{\sqrt{k\tilde{k}_z}}\mathrm{E}_{\varphi}^{d,p}(\rho_p,\varphi_p) = \frac{f_2}{f_1}\sqrt{\frac{k_z}{\tilde{k}_z}}\frac{e^{ik_z f_1}}{2i\epsilon_0 n^2 k_z}k^2\mathbf{P}^d\cdot\widehat{\mathbf{s}},\end{aligned} \tag{30}$$

with

$$\rho_p = f_2\frac{\tilde{k}_{\perp}}{k},\quad \rho_p\cos\varphi_p = -f_2\frac{\tilde{k}_x}{k},\quad \rho_p\sin\varphi_p = -f_2\frac{\tilde{k}_y}{k}, \tag{31}$$

where the wavenumber $k = \tilde{k}$, as the two lenses are in the same medium.

The numerical aperture NA_2 of the lens L_2 before the detector is smaller than that of the objective lens L_1, but the pupils of both lenses are identical. Hence the focal lengths of the two lenses are different. This implies the following relationship between the wave vectors of corresponding plane waves on the object side of lens L_1 and the image side of lens L_2:

$$k_{\perp} = \frac{f_2}{f_1}\tilde{k}_{\perp},\quad k_z = \sqrt{k^2-(f_2/f_1)^2\tilde{k}_{\perp}^2}. \tag{32}$$

By substituting Eq. (30) into Eq. (4), the electric field in image space becomes:

$$\begin{aligned}\mathbf{E}^{(i)}(\mathbf{r}) &= \frac{1}{4\pi^2}\left[\iint_{\tilde{k}_{\perp}\le k_0\mathrm{NA}_2}\left(\tilde{A}_p^d(\tilde{\mathbf{k}}_{\perp})\widehat{\mathbf{p}}(\tilde{\mathbf{k}}_{\perp})+\tilde{A}_s^d(\tilde{\mathbf{k}}_{\perp})\widehat{\mathbf{s}}(\tilde{\mathbf{k}}_{\perp})\right)e^{i\tilde{\mathbf{k}}\cdot\mathbf{r}}d^2\tilde{k}_{\perp}\right]\cdot\mathbf{P}^d\\ &= \frac{k^2 f_2}{4\pi i\epsilon_0 n^2 f_1}\left[\iint_{\tilde{k}_{\perp}\le k_0\mathrm{NA}_2}\frac{1}{\sqrt{k_z\tilde{k}_z}}\left(\widehat{\mathbf{p}}(\tilde{\mathbf{k}}_{\perp})\otimes\widehat{\mathbf{p}}\left(\frac{f_2}{f_1}\tilde{\mathbf{k}}_{\perp}\right)+\widehat{\mathbf{s}}(\tilde{\mathbf{k}}_{\perp})\otimes\widehat{\mathbf{s}}\left(\frac{f_2}{f_1}\tilde{\mathbf{k}}_{\perp}\right)\right)\right.\\ &\qquad\left.\cdot\, e^{ik_z f_1}e^{i\tilde{\mathbf{k}}\cdot\mathbf{r}}d^2\tilde{k}_{\perp}\right]\cdot\mathbf{P}^d,\end{aligned} \tag{33}$$

where

$$\begin{aligned}\widehat{\mathbf{p}}(\tilde{\mathbf{k}}_{\perp}) &= \frac{1}{k^2\tilde{k}_{\perp}}\begin{pmatrix}\tilde{k}_x\tilde{k}_z\\ \tilde{k}_y\tilde{k}_z\\ -\tilde{k}_{\perp}^2\end{pmatrix},\qquad \widehat{\mathbf{p}}\left(\frac{f_2}{f_1}\tilde{\mathbf{k}}_{\perp}\right) = \frac{1}{k^2\tilde{k}_{\perp}}\begin{pmatrix}\tilde{k}_x k_z\\ \tilde{k}_y k_z\\ -\frac{f_2}{f_1}\tilde{k}_{\perp}^2\end{pmatrix},\\ \widehat{\mathbf{s}}(\tilde{\mathbf{k}}_{\perp}) &= \widehat{\mathbf{s}}\left(\frac{f_2}{f_1}\tilde{\mathbf{k}}_{\perp}\right) = \frac{1}{k^2\tilde{k}_{\perp}}\begin{pmatrix}-\tilde{k}_y\\ \tilde{k}_x\\ 0\end{pmatrix},\end{aligned} \tag{34}$$

Using polar coordinates, the field in the image space can be written as:

$$\begin{aligned}E_x^{(i)}(\rho,\varphi,z) &= \frac{-f_2}{2\epsilon_0 n^2 f_1}\left[(K_{00}^0+K_{zz}^0)\mathbf{p}_x^{dip}-2iK_{\perp z}^1\cos\varphi\mathbf{p}_z^{dip}+(K_{00}^2-K_{zz}^2)(\cos 2\varphi\mathbf{p}_x^{dip}+\sin 2\varphi\mathbf{p}_y^{dip})\right],\\ E_y^{(i)}(\rho,\varphi,z) &= \frac{-f_2}{2\epsilon_0 n^2 f_1}\left[(K_{00}^0+K_{zz}^0)\mathbf{p}_y^{dip}-2iK_{\perp z}^1\sin\varphi\mathbf{p}_z^{dip}+(K_{00}^2-K_{zz}^2)(\sin 2\varphi\mathbf{p}_x^{dip}-\cos 2\varphi\mathbf{p}_y^{dip})\right],\\ E_z^{(i)}(\rho,\varphi,z) &= \frac{-f_2}{2\epsilon_0 n^2 f_1}\left[2K_{\perp\perp}^0\mathbf{p}_z^{dip}-2iK_{zz}^1(\cos\varphi\mathbf{p}_x^{dip}+\sin\varphi\mathbf{p}_y^{dip})\right],\end{aligned} \tag{35}$$

Optics EXPRESS

where

$$K_{00}^{n}(\rho,z)=\int_{0}^{k_0\mathrm{NA}_2}\left(\frac{\tilde{k}_z}{k}\right)^{1/2}\frac{\tilde{k}_\perp}{k\sqrt{k^2-(f_2/f_1)^2\tilde{k}_\perp^2}}\mathrm{J}_n(\tilde{k}_\perp\rho)e^{i\tilde{k}_z z}\cdot e^{iz\sqrt{k^2-(f_2/f_1)^2\tilde{k}_\perp^2}}d\tilde{k}_\perp,$$
$$K_{\perp\perp}^{n}(\rho,z)=\int_{0}^{k_0\mathrm{NA}_2}\left(\frac{\tilde{k}_z}{k}\right)^{1/2}\frac{\tilde{k}_\perp}{k\sqrt{k^2-(f_2/f_1)^2\tilde{k}_\perp^2}}q_{\perp\perp}(\tilde{k}_\perp)\mathrm{J}_n(\tilde{k}_\perp\rho)e^{i\tilde{k}_z z}\cdot e^{iz\sqrt{k^2-(f_2/f_1)^2\tilde{k}_\perp^2}}d\tilde{k}_\perp,$$
$$K_{\perp z}^{n}(\rho,z)=\int_{0}^{k_0\mathrm{NA}_2}\left(\frac{\tilde{k}_z}{k}\right)^{1/2}\frac{\tilde{k}_\perp}{k\sqrt{k^2-(f_2/f_1)^2\tilde{k}_\perp^2}}q_{\perp z}(\tilde{k}_\perp)\mathrm{J}_n(\tilde{k}_\perp\rho)e^{i\tilde{k}_z z}\cdot e^{iz\sqrt{k^2-(f_2/f_1)^2\tilde{k}_\perp^2}}d\tilde{k}_\perp,$$
$$K_{zz}^{n}(\rho,z)=\int_{0}^{k_0\mathrm{NA}_2}\left(\frac{\tilde{k}_z}{k}\right)^{1/2}\frac{\tilde{k}_\perp}{k\sqrt{k^2-(f_2/f_1)^2\tilde{k}_\perp^2}}q_{zz}(\tilde{k}_\perp)\mathrm{J}_n(\tilde{k}_\perp\rho)e^{i\tilde{k}_z z}\cdot e^{iz\sqrt{k^2-(f_2/f_1)^2\tilde{k}_\perp^2}}d\tilde{k}_\perp, \tag{36}$$

with $\tilde{k}_\perp=\sqrt{\tilde{k}_x^2+\tilde{k}_y^2}$, $\tilde{k}_z=\sqrt{k^2-\tilde{k}_\perp^2}$, and

$$q_{\perp\perp}(\tilde{k}_\perp)=\frac{k_\perp\tilde{k}_\perp}{k^2},\quad q_{\perp z}(\tilde{k}_\perp)=\frac{k_\perp\tilde{k}_z}{k^2},\quad q_{zz}(\tilde{k}_\perp)=\frac{k_z\tilde{k}_z}{k^2}. \tag{37}$$

We introduced the term $(\frac{\tilde{k}_z}{k})^{1/2}$ to account for an aplanatic lens.

2.3. Imaging with a polarization convertor

The longitudinal component cannot be easily measured by the detector. Furthermore, at the center of the detector the radial component is weaker than the longitudinal component. To detect the longitudinal component, we add a polarization convertor [26] between the collimator lens and the detector lens, which transforms the radially polarized light into x-polarized light before being refocused by the detector lens. As only x-polarized light needs to be measured by the detector, we put a polarizer in front of the detector as seen in Fig. 1(c). Then, the field in image space after the convertor and the polarizer becomes

$$\mathbf{E}^{(i),p}(\rho_p,\varphi_p)=E_\rho^{d,p}(\rho_p,\varphi_p)\widehat{\mathbf{x}}, \tag{38}$$

Due to the convertor, the radial and azimuthal components of the field in the entrance pupil of the second lens become:

$$E_\rho^{(i),p}(\rho_p,\varphi_p)=E_\rho^{d,p}(\rho_p,\varphi_p)\cos\phi,\quad E_\varphi^{(i),p}(\rho_p,\varphi_p)=-E_\rho^{d,p}(\rho_p,\varphi_p)\sin\phi. \tag{39}$$

The vector amplitudes of the plane waves in image space corresponding to the pupil field have p- and s- components are given by:

$$\tilde{A}_\mathrm{p}(\tilde{\mathbf{k}}_\perp)=\frac{2\pi i f_2}{\sqrt{\tilde{k}\tilde{k}_z}}\mathrm{E}_\rho^{(i),p}(\rho_p,\varphi_p),\quad \tilde{A}_\mathrm{s}(\tilde{\mathbf{k}}_\perp)=\frac{2\pi i f_2}{\sqrt{\tilde{k}\tilde{k}_z}}\mathrm{E}_\varphi^{(i),p}(\rho_p,\varphi_p), \tag{40}$$

Optics EXPRESS

Substituting Eq. (40) into Eq. (4) and using polar coordinates, finally, gives for the field in image space can be deduced as:

$$
\begin{aligned}
E_x^{(i)}(\rho,\varphi,z) &= \frac{-f_2}{2\epsilon_0 n^2 f_1}\Big[\frac{i}{2}(K_{zz}^3 - K_z^3)(\cos 3\varphi \mathbf{p}_x^{dip} + \sin 3\varphi \mathbf{p}_y^{dip}) - \frac{i}{2}K_{zz}^1(3\cos\varphi \mathbf{p}_x^{dip} + \sin\varphi \mathbf{p}_y^{dip}) \\
&\quad - \frac{i}{2}K_z^1(\cos\varphi \mathbf{p}_x^{dip} + 3\sin\varphi \mathbf{p}_y^{dip}) - (K_{\perp z}^2 - K_\perp^2)\cos 2\varphi \mathbf{p}_z^{dip} + (K_{\perp z}^0 + K_\perp^0)\mathbf{p}_z^{dip}\Big], \\
E_y^{(i)}(\rho,\varphi,z) &= \frac{-f_2}{2\epsilon_0 n^2 f_1}\Big[\frac{i}{2}(K_{zz}^3 - K_z^3)(\sin 3\varphi \mathbf{p}_x^{dip} - \cos 3\varphi \mathbf{p}_y^{dip}) - \frac{i}{2}(K_{zz}^1 - K_z^1)(\sin\varphi \mathbf{p}_x^{dip} + \cos\varphi \mathbf{p}_y^{dip}) \\
&\quad - (K_{\perp z}^2 - K_\perp^2)\sin 2\varphi \mathbf{p}_z^{dip}\Big], \\
E_z^{(i)}(\rho,\varphi,z) &= \frac{-f_2}{2\epsilon_0 n^2 f_1}\Big[-K_{z\perp}^0 \mathbf{p}_x^{dip} + K_{z\perp}^2(\cos 2\varphi \mathbf{p}_x^{dip} + \sin 2\varphi \mathbf{p}_y^{dip}) + 2iK_{\perp\perp}^1\cos\varphi \mathbf{p}_z^{dip}\Big],
\end{aligned}
\tag{41}
$$

where

$$
\begin{aligned}
K_{z\perp}^n(\rho,z) &= \int_0^{k_0\mathrm{NA}_2}\left(\frac{\tilde{k}_z}{k}\right)^{1/2}\frac{\tilde{k}_\perp}{k\sqrt{k^2-(f_2/f_1)^2\tilde{k}_\perp^2}}q_{z\perp}(\tilde{k}_\perp)\mathrm{J}_n(\tilde{k}_\perp\rho)e^{i\tilde{k}_z z}\cdot e^{iz\sqrt{k^2-(f_2/f_1)^2\tilde{k}_\perp^2}}d\tilde{k}_\perp, \\
K_z^n(\rho,z) &= \int_0^{k_0\mathrm{NA}_2}\left(\frac{\tilde{k}_z}{k}\right)^{1/2}\frac{\tilde{k}_\perp}{k\sqrt{k^2-(f_2/f_1)^2\tilde{k}_\perp^2}}q_z(\tilde{k}_\perp)\mathrm{J}_n(\tilde{k}_\perp\rho)e^{i\tilde{k}_z z}\cdot e^{iz\sqrt{k^2-(f_2/f_1)^2\tilde{k}_\perp^2}}d\tilde{k}_\perp, \\
K_\perp^n(\rho,z) &= \int_0^{k_0\mathrm{NA}_2}\left(\frac{\tilde{k}_z}{k}\right)^{1/2}\frac{\tilde{k}_\perp}{k\sqrt{k^2-(f_2/f_1)^2\tilde{k}_\perp^2}}q_\perp(\tilde{k}_\perp)\mathrm{J}_n(\tilde{k}_\perp\rho)e^{i\tilde{k}_z z}\cdot e^{iz\sqrt{k^2-(f_2/f_1)^2\tilde{k}_\perp^2}}d\tilde{k}_\perp,
\end{aligned}
\tag{42}
$$

where

$$
q_{z\perp}(\tilde{k}_\perp) = \frac{k_z\tilde{k}_\perp}{k^2}, \quad q_\perp(\tilde{k}_\perp) = \frac{k_\perp}{k}, \quad q_z(\tilde{k}_\perp) = \frac{k_z}{k}. \tag{43}
$$

and $k_\perp$ and k_z are functions of $\tilde{k}_\perp$ given by Eq. (32). Other symbols are shown in Eq. (37). Again, we introduced the term $(\frac{\tilde{k}_z}{k})^{1/2}$ to account for an aplanatic lens.

3. Numerical results

Through this section, we assume the light with wavelength $\lambda = 500nm$. With Eq. (11) and (17), the focal fields of linearly and radially polarized illumination can be obtained. It follows for Fig. 2 that the FWHM of the electric energy density $|\vec{\mathbf{E}}|^2$ in the focal plane of the radially polarized pupil field, is slightly smaller than that of a linearly pupil field ($\mathrm{FWHM}_{total}^{rad} \approx 0.72\lambda, \mathrm{FWHM}_{total}^{lin} \approx 0.76\lambda$). In contrast, the FWHM of the squared modulus of the longitudinal component corresponding to the radially polarized pupil field ($\mathrm{FWHM}_{long}^{rad} = 0.48\lambda$), is much smaller than the FWHM of $|\vec{\mathbf{E}}|$ in the case of a linearly polarized pupil field. Thus, the polarization state of the light strongly influences the size of the focused spot in the case of high NA. If the sample is sensitive only to the longitudinal component of the focal spot, then the use of radially polarized light can result in a substantial improvement in resolution.

Figure 3 shows the comparison of the squared amplitude of the longitudinal component of the focal spots obtained in the case of radially polarized illumination with full aperture, annular aperture and optimized radially polarized illumination, as described in Eqs. (17)-(24). The

Optics EXPRESS

optimized pupil field has FWHM which is 5.4% smaller than that of the full aperture constant pupil field. The FWHM of the squared amplitude of the longitudinal component obtained by focusing a radially polarized beam using a ring mask function (with radius 90% of the total pupil) is even smaller than the above two cases. However, the expanding side lobes in the annular case is larger than for the full aperture and the optimized case. But the energy in the focal region is of course much weaker in the annular case.

We use expressions Eq. (35) and (41) (with/without a polarization convertor) to compute the normalized detector signal. In order to make full use of the longitudinal component, the electric dipole is set along the z-axis. A small pinhole is taken into consideration in the confocal system [32]. The criterion for choosing a suitable pinhole size is to make an aperture giving 50% of the maximum intensity [33].

As is indicated in Fig. 1, we detect the intensity with a single-pixel camera at the focal point

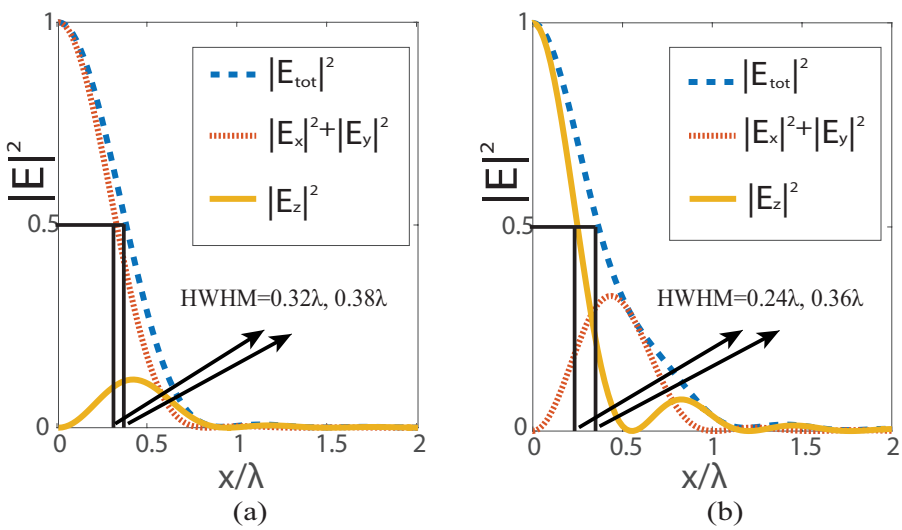

Fig. 2. Profiles of the squared amplitude of the longitudinal and transverse components and total energy density $|\vec{\mathbf{E}}|^2$ in the focal plane in the case of a pupil field that is linearly polarized in the $x-$ direction (a) and a pupil field that is radially polarized (b). The focusing lens has NA=0.9. The plots are normalized to the on-axis peak values.

of the detector lens, which is located at $r = (0, 0, 0)$. However, if we assume purely longitudinal dipole excitation, then without polarization conversion, the intensity at the focal point is a local minimum, meaning that very little intensity is detected. To solve this problem, we propose to use a polarization convertor in the pupil of the lens L_2 to change the radially polarized light to linearly polarized light, which in the focal plane will result in an intensity distribution with its maximum at the focal point. The intensity at the detector plane can be obtained by Eq. (41). Figure 4 shows the final signal along the x axis when the pinhole is set before the detector and the dipole is scanned in the x-y plane at the object plane. Note that because of the use of the polarization convertor, the original radial polarization is turned into linear polarization and thus the "transversal" component in Fig. 4 corresponds to the contribution of the radially polarized light emitted by the dipole.

To validate that the system has the advantage of higher resolution, two dipoles close to each other need to be analyzed with the above theory. Figure 5 shows the cross sections of the detected intensity when two dipoles that are parallel are scanned by a focused spot. The polarization of the illumination is taken as either linear, radial or optimized radial as shown in

Optics EXPRESS

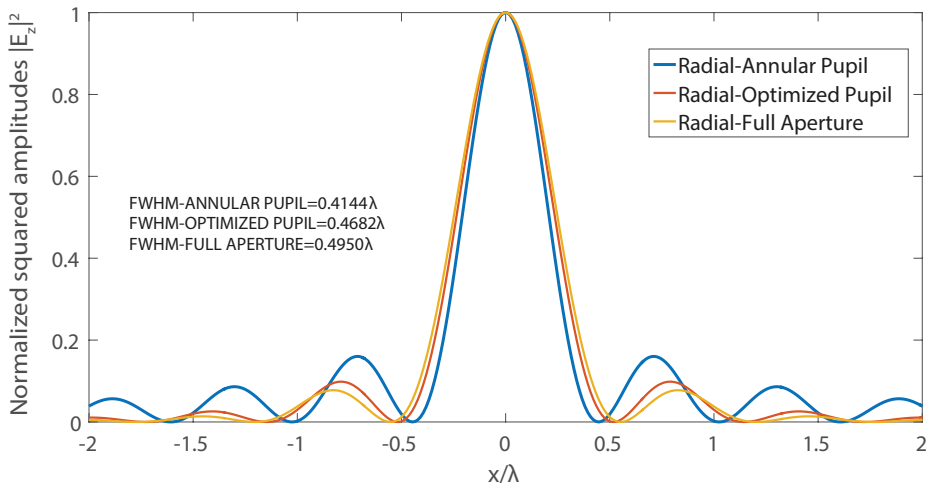

Fig. 3. Profiles of the squared amplitudes of the longitudinal components of the exciting spot in the focal plane in the case of radially polarized illumination with full aperture, annular aperture and optimized radially polarized pupil field. The plots are normalized to their on-axis maxima.

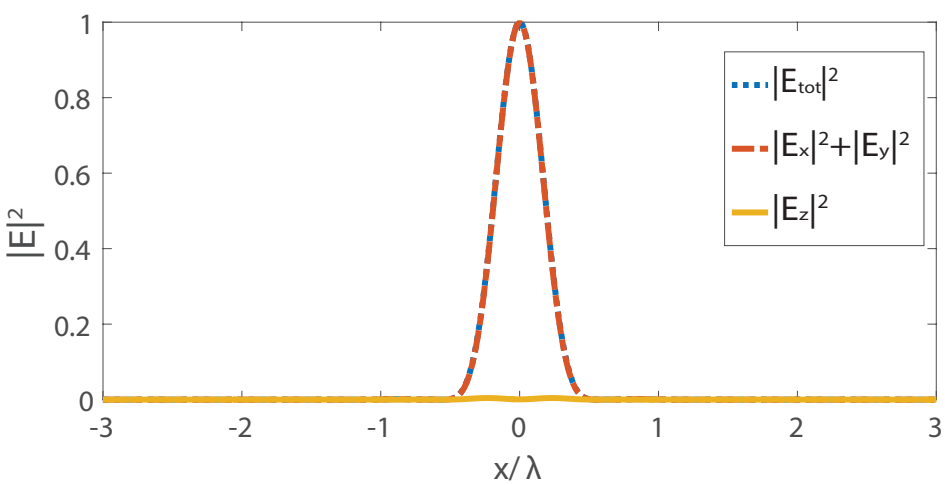

Fig. 4. Profiles of the intensities at the detector plane with a polarization convertor and a small pinhole with radius $r = 0.18\mu m$ which is 0.36λ in terms of wavelength. The system is composed of: a high $NA_1 = 0.9$ focusing objective lens and a low $NA_2 = 0.3$ lens for detection. For illumination, radially polarized light of wavelength $\lambda = 500nm$ is used. The focal field can be seen in Eq. (17). The dipole is set rigidly along the $z-$axis direction (only α_{zz} is relevant). The plots are normalized to on-axis maxima.

Optics EXPRESS

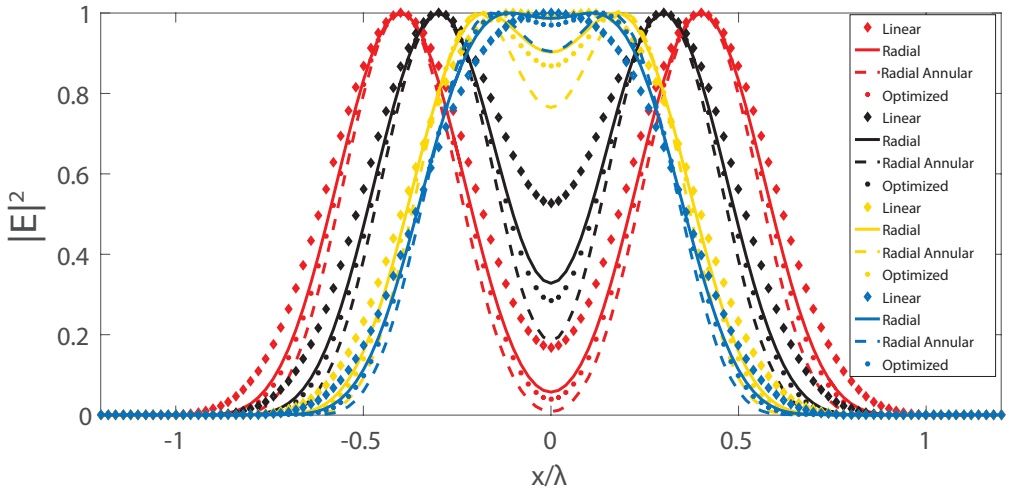

Fig. 5. Profiles of the detected intensities as function of scanning distance of two separated dipoles for different kinds of illumination and for several distances between the dipoles. The system is composed of two lenses with $\mathrm{NA}_1 = 0.9$, and $\mathrm{NA}_2 = 0.3$ and is illuminated by light with a wavelength of $\lambda = 500nm$. The illumination is either linearly, radially or optimized radially polarized. The two dipoles are set along the x axis for the linear polarization and along the z axis for the other radially polarized cases. A polarization convertor is added in the case of radially polarized excitation. Four different distances between the dipoles are chosen: d=0.8λ (red line), d=0.6λ (black line), d=0.4λ (yellow line), and d=0.36λ (blue line). The plots are normalized to the on-axis peak intensity.

Eq. (11) and (17)-(24). For linearly x-polarized illumination (diamond dot line), the dipoles are set along the x-axis (only α_{xx} is relevant). If we want to roughly distinguish the two dipoles, the distance between them should be larger than 0.6λ according to the Rayleigh criterion. This value is approaching the diffraction limit $0.61\frac{\lambda}{\mathrm{NA}}$. However, for normal radial illumination (solid line), radial illumination with a ring mask (dashed line) and optimized radial illumination (dot line), with the dipoles set along the z-axis (only α_{zz} is relevant), the smallest distance at which they can be distinguished is reduced to 0.4λ. Meanwhile, the optimized one gives more obvious contrast than the normal radial case and the radial annular case gives the highest contrast. Even when the distance between the two dipoles decreases to 0.36λ, it can be seen that for the radial excitation with a ring mask and optimized radially polarized excitation, the two dipoles can be distinguished better than for the other two focused spots. Moreover, at this distance, note that in the case of linear polarization, the dipoles cannot be resolved.

The visibility as a function of d/λ can be seen in Fig. 6. Here the visibility is defined as:

$$\text{visibility} = \frac{I_{max} - I_{min}}{I_{max} + I_{min}}. \tag{44}$$

Here I_{max} is the normalized intensity which equals 1 and I_{min} is the value of the intensity at $r = (0, 0, 0)$ as shown in Fig. 5. When $d/\lambda > 1.2$, for the four cases, the two dipoles can be resolved very well. When $0.2 < d/\lambda < 1.2$, it is clearly seen that the visibility value of linear excitation is smaller than the other three cases, which means the worst resolution. While the visibility value of radial excitation with the annular objective is the highest in this range. When $0.2 < d/\lambda < 0.3$, the resolution of the system is almost the same for the three radially polarized light excitation cases. When $d/\lambda < 0.2$, the dipoles can not be resolved any more in all cases because of the diffraction limit. This property of visibility agrees well with Fig. 5.

Optics EXPRESS

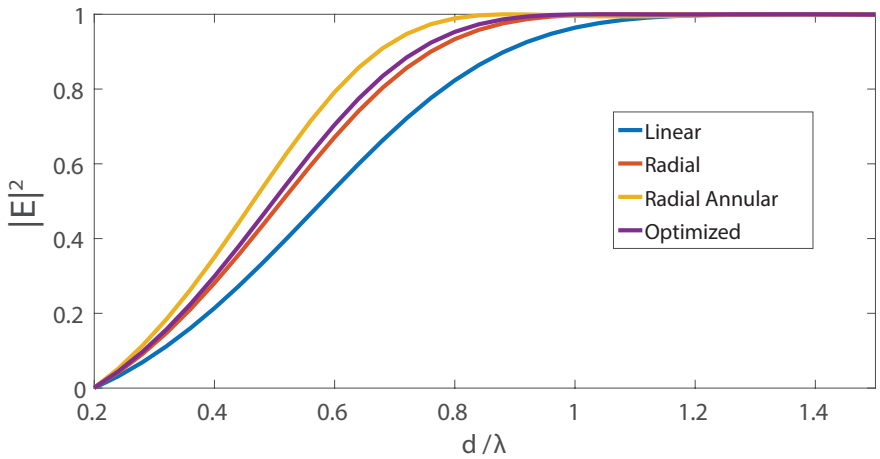

Fig. 6. Profiles of the visibility as a function of the d/λ for the four cases of pupil fields. The system is the same as shown in Fig. 5.

4. Conclusion

To conclude, we present a complete vectorial theoretical analysis to describe the whole imaging process of the high NA confocal system from the illumination point to the imaging plane. Strong longitudinal component as well as shaper focal spots are achieved by comparing the linear ($\mathrm{FWHM}^{lin}_{total} \approx 0.76\lambda$) and radial ($\mathrm{FWHM}^{rad}_{total} \approx 0.72\lambda$) polarization pupil fields. In order to obtain the higher resolution, we apply an optimized pupil field with an amplitude distribution that varies monotonically in the radial direction, which provides 5.4% tighter focused spot for NA = 0.9 than the full aperture constant pupil field. Additionally, the condition of radially polarized illumination with an annular objective lens is also considered to provide the smallest focal spot size, although at the expense of expanding side lobes.

Four kinds of focused spots are used to scan two parallel longitudinal dipoles with variable distances in the objective plane. In order to efficiently detect the field scattered by the longitudinally oriented dipoles, we insert a radial to linear polarization convertor before the pinhole. From our analysis, we show that for a pinhole in front of the detector with radius 0.36λ, by using a radial pupil field with the an annular lens to excite the dipoles, a distance of 0.36λ can be resolved, i.e., beyond the diffraction limit. The proposed method is easy to apply to other pupil fields and helpful to analyze confocal systems. The experiment can be conducted on the basis of the theory and simulated results with different samples to validate the superiority of the optimized radially polarized illumination combined with the confocal system.

References

1. S. W. Hell and J. Wichmann, "Breaking the diffraction resolution limit by stimulated emission: stimulated-emission-depletion fluorescence microscopy," Opt. Lett. **19**, 780–782 (1994).
2. E. Betzig, G. H. Patterson, R. Sougrat, O. W. Lindwasser, S. Olenych, J. S. Bonifacino, M. W. Davidson, J. Lippincott-Schwartz, and H. F. Hess, "Imaging intracellular fluorescent proteins at nanometer resolution," Science **313**, 1642–1645 (2006).
3. M. J. Rust, M. Bates, and X. Zhuang, "Sub-diffraction-limit imaging by stochastic optical reconstruction microscopy (storm)," Nat. Methods **3**, 793 (2006).
4. D. V. Patel and C. N. McGhee, "Contemporary in vivo confocal microscopy of the living human cornea using white light and laser scanning techniques: a major review," Clin. Exp. Ophthalmol. **35**, 71–88 (2007).
5. A. Hoffman, M. Goetz, M. Vieth, P. Galle, M. Neurath, and R. Kiesslich, "Confocal laser endomicroscopy: technical status and current indications," Endoscopy **38**, 1275–1283 (2006).

Optics EXPRESS

6. S. Le Person, J. Puiggali, M. Baron, and M. Roques, "Near infrared drying of pharmaceutical thin films: experimental analysis of internal mass transport," Chem. Eng. Process. Process. Intensif. **37**, 257–263 (1998).
7. S. Götzinger, L. de S Menezes, O. Benson, D. Talapin, N. Gaponik, H. Weller, A. Rogach, and V. Sandoghdar, "Confocal microscopy and spectroscopy of nanocrystals on a high-q microsphere resonator," J. Opt. B **6**, 154 (2004).
8. K. Lindfors, T. Kalkbrenner, P. Stoller, and V. Sandoghdar, "Detection and spectroscopy of gold nanoparticles using supercontinuum white light confocal microscopy," Phys. Rev. Lett. **93**, 037401 (2004).
9. L. Novotny and B. Hecht, *Principles of nano-optics* (Cambridge University).
10. T. Wilson, R. Juškaitis, and P. Higdon, "The imaging of dielectric point scatterers in conventional and confocal polarisation microscopes," Opt. Commun. **141**, 298 – 313 (1997).
11. R. Dorn, S. Quabis, and G. Leuchs, "Sharper focus for a radially polarized light beam," Phys. Rev. Lett. **91**, 233901 (2003).
12. K. S. Youngworth and T. G. Brown, "Focusing of high numerical aperture cylindrical-vector beams," Opt. Express **7**, 77–87 (2000).
13. R. Chen, K. Agarwal, C. J. Sheppard, and X. Chen, "Imaging using cylindrical vector beams in a high-numerical-aperture microscopy system," Opt. Lett. **38**, 3111–3114 (2013).
14. S. Quabis, R. Dorn, M. Eberler, O. Glöckl, and G. Leuchs, "Focusing light to a tighter spot," Opt. Commun. **179**, 1 – 7 (2000).
15. C. J. Sheppard and A. Choudhury, "Annular pupils, radial polarization, and superresolution," Appl. Opt. **43**, 4322–4327 (2004).
16. L. Yang, X. Xie, S. Wang, and J. Zhou, "Minimized spot of annular radially polarized focusing beam," Opt. Lett. **38**, 1331–1333 (2013).
17. Y. Kozawa and S. Sato, "Focusing property of a double-ring-shaped radially polarized beam," Opt. Lett. **31**, 820–822 (2006).
18. H. Wang, L. Shi, B. Lukyanchuk, C. Sheppard, and C. T. Chong, "Creation of a needle of longitudinally polarized light in vacuum using binary optics," Nat. Photonics **2**, 501 (2008).
19. H. Guo, X. Weng, M. Jiang, Y. Zhao, G. Sui, Q. Hu, Y. Wang, and S. Zhuang, "Tight focusing of a higher-order radially polarized beam transmitting through multi-zone binary phase pupil filters," Opt. Express **21**, 5363–5372 (2013).
20. F. Tang, Y. Wang, L. Qiu, W. Zhao, and Y. Sun, "Super-resolution radially polarized-light pupil-filtering confocal sensing technology," Appl. Opt. **53**, 7407–7414 (2014).
21. N. Davidson and N. Bokor, "High-numerical-aperture focusing of radially polarized doughnut beams with a parabolic mirror and a flat diffractive lens," Opt. Lett. **29**, 1318–1320 (2004).
22. H. Urbach and S. Pereira, "Field in focus with a maximum longitudinal electric component," Phys. Rev. Lett. **100**, 123904 (2008).
23. K. Ushakova, Q. Van den Berg, S. Pereira, and H. Urbach, "Demonstration of spot size reduction by focussing amplitude modulated radially polarized light on a photoresist," J. Opt. **17**, 125615 (2015).
24. D. P. Biss, K. S. Youngworth, and T. G. Brown, "Dark-field imaging with cylindrical-vector beams," Appl. Opt. **45**, 470–479 (2006).
25. W. T. Tang, E. Y. Yew, and C. J. Sheppard, "Polarization conversion in confocal microscopy with radially polarized illumination," Opt. Lett. **34**, 2147–2149 (2009).
26. X. Xie, Y. Chen, K. Yang, and J. Zhou, "Harnessing the point-spread function for high-resolution far-field optical microscopy," Phys. Rev. Lett. **113**, 263901 (2014).
27. V. Ignatowsky, "Diffraction by a lens of arbitrary aperture," Trans. Opt. Inst **1**, 1–36 (1919).
28. E. Wolf, "Electromagnetic diffraction in optical systems. i. an integral representation of the image field," in *Proc. Royal Soc. London A: Math. Phys. Eng. Sci.*, vol. **253** (The Royal Society, 1959), pp. 349–357.
29. B. Richards and E. Wolf, "Electromagnetic diffraction in optical systems. ii. structure of the image field in an aplanatic system," in *Proc. Royal Soc. London A: Math. Phys. Eng. Sci.*, vol. **253** (The Royal Society, 1959), pp. 358–379.
30. M. Abramowitz and I. A. Stegun, *Handbook of mathematical functions: with formulas, graphs, and mathematical tables*, vol. 55 (Courier Corporation).
31. J. Jackson, *Classical Electrodynamics, 2nd ed.* (John Wiley & Sons).
32. P. Török, P. Higdon, and T. Wilson, "Theory for confocal and conventional microscopes imaging small dielectric scatterers," J. Mod. Opt. **45**, 1681–1698 (1998).
33. D. B. Murphy, *Fundamentals of Light Microscopy and Electronic Imaging* (John Wiley & Sons).